INTERNATIONAL JOURNAL FOR NUMERICAL METHODS IN FLUIDS, VOL. 20, 363–391 (1995)

A TRANSPORT APPROACH TO THE CONVOLUTION METHOD FOR NUMERICAL MODELLING OF LINEARIZED 3D CIRCULATION IN SHALLOW SEAS

ZHIGANG XU

Department of Oceanography, Dalhousie University, Halifax, N.S., Canada B3H 4J1

SUMMARY

A new method for solving the linearized equations of motion is presented in this paper, which is the implementation of an outstanding idea suggested by Welander: a transport approach to the convolution method. The present work focuses on the case of constant eddy viscosity and constant density but can be easily extended to the case of arbitrary but time-invariant eddy viscosity or density structure. As two of the three equations of motion are solved analytically and the main numerical 'do-loop' only updates the sea level and the transport, the method features succinctness and fast convergence.

The method is tested in Heaps' basin and the results are compared with Heaps' results for the transient state and with analytical solutions for the steady state. The comparison yields satisfactory agreement. The computational advantage of the method compared with Heaps' spectral method and Jelesnianski's bottom stress method is analysed and illustrated with examples.

Attention is also paid to the recent efforts made in the spectral method to accelerate the convergence of the velocity profile. This study suggests that an efficient way to accelerate the convergence is to extract both the wind-induced surface Ekman spiral and the pressure-induced bottom Ekman spiral as a prespecified part of the profile.

The present work also provides a direct way to find the eigenfunctions for arbitrary eddy viscosity profile. In addition, mode-truncated errors are analysed and tabulated as functions of mode number and the ratio of the Ekman depth to the water depth, which allows a determination of a proper mode number given an error tolerance.

KEY WORDS transport approach; convolution method; linearized 3D circulation; shallow water equations

1. INTRODUCTION

The set of linearized equations

$$\begin{aligned}
&\frac{\partial u}{\partial t} - fv = -g\,\frac{\partial \eta}{\partial x} + \frac{\partial}{\partial z}\left(\upsilon\,\frac{\partial u}{\partial z}\right),\\
&\frac{\partial v}{\partial t} + fu = -g\,\frac{\partial \eta}{\partial y} + \frac{\partial}{\partial z}\left(\upsilon\,\frac{\partial v}{\partial z}\right),\\
&\frac{\partial \eta}{\partial t} + \frac{\partial}{\partial x}\int_{-h}^{0} u\,\mathrm{d}z + \frac{\partial}{\partial y}\int_{-h}^{0} v\,\mathrm{d}z = 0,
\end{aligned} \tag{1}$$

where x–y–z forms a right-handed Cartesian co-ordinate system, t is time, u and v are the velocity components in the x- and y-directions respectively, η is the sea surface elevation, f is the Coriolis parameter, υ is the eddy viscosity and g is the gravitational acceleration, has often been used as a mathematical model for tidal flow, storm surge prediction, shelf circulation, etc. The set, however,

CCC 0271–2091/95/050363–29

Received 4 October 1993
Revised 23 July 1994

rarely has a full ($\sim f(t, x, y, z)$) analytical solution, even for very simple basins. Although it has been greatly simplified from the full Navier–Stokes equations, it still includes a mixture of Ekman dynamics and long-wave dynamics. Therefore it is necessary to take a numerical approach to obtain general solutions.

However, before integrating the equations numerically, we may be able to extract the Ekman dynamics analytically. This is actually an idea proposed by Welander.[1] Specifically, he suggested that the two momentum equations can be solved for a complex velocity $q = u + iv$ in terms of a known wind stress τ and an unknown sea surface slope, $\nabla\eta$:

$$q = q(t, z; \nabla\eta, \tau). \tag{2}$$

As we will see later, equation (2) can be written in the form of a pair of time convolutions. One convolves the wind forcing with a wind response kernel and the other convolves the slope forcing with a pressure response kernel. In practice the wind stress is given. If the slope forcing were given, then the knowledge of the velocity field would be complete. To get $\nabla\eta(t)$, Welander[1] suggested two approaches (Table I). One is to take the derivative of q with respect to z and evaluate it at the bottom to get an analytical expression for a bottom stress. The bottom stress can then be substituted into a set of depth-averaged equations to numerically solve for η and the depth-averaged velocity components, $\bar{u}$ and $\bar{v}$. The other way is to integrate q over the water column to get a transport. The transport can then be

Table I. This table summarizes Welander's two suggestions $q_d(t, z; I_\tau)$ and $q_s(t, z; I_{\nabla\gamma})$ are two flows induced by unit constant wind stress I_τ and unit sea surface slope $I_{\nabla\gamma}$. A unit vector here is defined as a vector whose length is one unit and whose angle is zero. The dots on q_a and q_d indicate the time derivatives on them

$$\left.\begin{aligned} \frac{\partial u}{\partial t} - fv &= -g\frac{\partial \eta}{\partial x} + \upsilon\frac{\partial^2 u}{\partial z^2} \\ \frac{\partial v}{\partial t} + fu &= -g\frac{\partial \eta}{\partial y} + \upsilon\frac{\partial^2 u}{\partial z^2} \end{aligned}\right\} \quad \Rightarrow \quad \left\{ q = \nabla\eta * \dot{q}_s(t, z; I_{\nabla\eta}) + \tau * \dot{q}_d(t, z; I_\tau) \right.$$

$$\downarrow \qquad \downarrow$$

Jelesnianski's bottom stress approach — 1 — 2

$$\left.\begin{aligned} \frac{\partial \bar{u}}{\partial t} + \frac{\partial h\bar{u}}{\partial x} + \frac{\partial h\bar{v}}{\partial y} &= 0 \\ \frac{\partial \bar{u}}{\partial t} - f\bar{v} &= -g\frac{\partial \eta}{\partial x} + \frac{\tau_x^s - \tau_x^b}{h} \\ \frac{\partial \bar{v}}{\partial t} + f\bar{u} &= -g\frac{\partial \eta}{\partial y} + \frac{\tau_y^s - \tau_y^b}{h} \end{aligned}\right\} \quad \xrightarrow{\nabla\eta}$$

Welander's first suggestion (1)

$$\xrightarrow{(\tau_x^b, \tau_y^b)} \quad \left\{ \left(\tau_x^b, \tau_y^b\right) = \nabla\eta * \left.\frac{\partial \dot{q}_s}{\partial z}\right|_{z=-h} + \tau * \left.\frac{\partial \dot{q}_d}{\partial z}\right|_{z=-h} \right.$$

This study's transport approach — Welander's second suggestion (2)

$$\left.\frac{\partial \eta}{\partial t} + \frac{\partial h\bar{u}}{\partial x} + \frac{\partial h\bar{v}}{\partial y} = 0\right\} \quad \xrightarrow[(h\bar{u}, h, \bar{v})]{\nabla\eta} \quad \left\{ (h\bar{u}, h\bar{v}) = \nabla\eta * \int_{-h}^{0} \dot{q}_s \, dz + \tau * \int_{-h}^{0} \dot{q}_d \, dz \right.$$

substituted into the continuity equation to numerically solve for η. Both are variations of the convolution method. The difference between the two approaches lies in the way they supply the local forcing $\nabla\eta(t)$ for the convolution.

Welander[1] was interested in implementing the convolution method with the transport approach and planned to perform some numerical experiments for the North Sea. By 1961, however, he acknowledged a difficulty of the implementation because of the complexity of the integrodifferential equation.[2] The difficulty was also recognized by others.[3–5]

Jelesnianski[6] implemented the convolution method with the bottom stress approach and developed a model for storm surge prediction. Forristall[7–9] applied Jelesnianski's method to model storm-generated currents and later extended the method to the case of two layers of different but constant eddy viscosity. Davies[10,11] pushed this method one step further to the case of a non-linear depth-averaged model, using the bottom stress derived from a linear depth-dependent model to provide closure for the non-linear depth-averaged model. A difficulty with the bottom stress approach is the extremely slow convergence of the bottom stress series. Therefore approximate formulae have been used to replace the bottom stress series in this approach.[12,13] Such approximations, owing to the underestimation of the correct bottom stress, tend to produce the undamped inertial oscillations reported by Davies[10] and Hearn and Hunter.[12]

This study implements Welander's outstanding idea, resulting in a new method for numerical integration of the system (1). The new method features separation of the calculation for the surface elevation from that for the velocity. The separation results in a significant reduction of the computational workload owing to two factors. First, in calculating the elevation, only the transport series is involved, which requires fewer modes for its summing up than do the velocity series and the bottom stress series. Second, in calculating the velocity, both the wind-induced surface Ekman spiral and the slope-induced bottom Ekman spiral are extracted from the velocity series so that the remainder series converges exponentially. Section 4 will elaborate on these points.

Sheng and Thompson[14] propose a modification to Heaps' spectral method to accelerate the convergence of the velocity series. In their method the wind-induced surface Ekman spiral is extracted but the slope-induced bottom Ekman spiral is left in the series. It has become a topic of recent research interest to seek a better form for the prescribed part of the velocity so that the remainder converges faster.[14–18] Although the primary purpose of this paper is to implement Welander's idea, a section of this paper (Section 5) is therefore devoted to a discussion on this topic.

Owing to the inherent assumptions concerning the linearity of the system in question, the method is not extendable to fully non-linear problems. However, one may use perturbation techniques to extend the method to weakly non-linear problems in principle. In geophysical fluid problems with scales of 100–1000 km the Rossby number (an indication of the non-linearity; see e.g. Reference 19) is often small. As such, a linear system such as (1) can be a powerful model for many practical problems. This paper offers a new method for numerical integration of the system. The method cuts the computational workload substantially. This can be very valuable in problems requiring repeated integration of the system, such as data assimilation.

2. THE TRANSPORT APPROACH

This section gives a complete description of the transport approach for the case of constant density and constant eddy viscosity using either slip or non-slip bottom boundary conditions. Appendix II will discuss how to extend the method to the case of arbitrary but time-independent vertical profiles of eddy viscosity and density.

2.1. Extraction of Ekman dynamics

By Ekman dynamics we refer to the response of a local water column (in a Eulerian sense) to the wind stress applied at the surface and to the pressure gradient force exerted along the verticla sides. Under the assumptions of linearity, hydrostaticity, constant density and eddy viscosity and Coriolis parameter the response is governed by the two sets of equations

$$\begin{aligned} &\frac{\partial q_d}{\partial t} + ifq_d - \upsilon \frac{\partial^2 q_d}{\partial z^2} = 0, \\ &\upsilon \frac{\partial q_d}{\partial z}\bigg|_{z=0} = \tau(t), \qquad \left(\upsilon \frac{\partial q}{\partial z} - kq_d\right)_{z=-h} = 0, \\ &q_d|_{t=0} = 0 \end{aligned} \tag{3}$$

and

$$\begin{aligned} &\frac{\partial q_s}{\partial t} + ifq_s - \upsilon \frac{\partial^2 q_s}{\partial z^2} = -g\nabla\eta(t), \\ &\upsilon \frac{\partial q_s}{\partial z}\bigg|_{z=0} = 0, \qquad \left(\upsilon \frac{\partial q}{\partial z} - kq_s\right)_{z=-h} = 0, \\ &q_s|_{t=0} = 0, \end{aligned} \tag{4}$$

where q_d is a complex drift current induced by the wind, q_s is a complex slope current induced by the sea surface slope and k is a constant coefficient. An infinite k corresponds to the non-slip bottom condition.

Our task is to find solutions to these equations, which can be done in two different ways. One is to solve the equations numerically given the values of $\tau(t)$ and $\nabla\eta(t)$ at each new time step. This is essentially the philosophy behind Lardner's VHS (vertical and horizontal split) method.[20,21] Alternatively, it is well known that for a linear system, it we know its response to unit constant force, we can know its reponse to any force. This paper uses the second approach.

By replacing the two arbitrary forces $\tau(t)$ and $\nabla\eta(t)$ in (3) and (4) by two special forces—a constant unit wind stress I_τ, and a constant unit sea surface slope I_η—one can easily find the two solutions

$$q_d(t,\ z;\ I_\tau) = \frac{I_\tau}{f\delta_e}\left(SE(z) - \sum_{n=0}^{\infty} a_n\, e^{-b_n t}\, \cos(\omega_n z)\right), \tag{5}$$

$$q_s(t,\ z;\ I_\eta) = i\,\frac{gI_\eta}{f}\left(BE(z) - \sum_{n=0}^{\infty} c_n\, e^{-b_n t}\, \cos(\omega_n z)\right), \tag{6}$$

where

$$SE(z) = \sqrt{2}\, e^{-i\pi/4}\, \frac{\sinh[\alpha(h+z)] + (\alpha\upsilon/k)\, \cosh[\alpha(h+z)]}{\cosh(\alpha h) + (\alpha\upsilon/k)\, \sinh(\alpha h)} \quad \text{(surface Ekman spiral)}, \tag{7}$$

$$BE(z) = 1 - \frac{\cosh(\alpha z)}{\cosh(\alpha h) + (\alpha\upsilon/k)\, \sinh(\alpha h)} \quad \text{(bottom Ekman spiral)}, \tag{8}$$

$$\delta_e = \sqrt{\left(\frac{2\upsilon}{f}\right)} \quad \text{(Ekman depth)}, \tag{9}$$

$$\alpha = \sqrt{\left(\frac{if}{\upsilon}\right)} \quad \text{or} \quad \frac{1+i}{\delta_e}, \tag{10}$$

$$\beta_n = \frac{\omega_n h}{\sqrt{2}} \frac{\delta_e}{h}, \tag{11}$$

$$a_n = \frac{\delta_e}{h} \frac{4}{\left[(\omega_n h)^2(\delta_e/h)^2+2i\right](1+\varepsilon_n)}, \tag{12}$$

$$b_n = \left[\frac{(\omega_n h)^2}{2}\left(\frac{\delta_e}{h}\right)^2+i\right]f, \tag{13}$$

$$c_n = i \frac{4 \sin(\omega_n h)}{\omega_n h\left[(\omega_n h)^2(\delta_e/h)^2+2i\right](1+\varepsilon_n)}. \tag{14}$$

The ω_n are the roots of

$$\omega_n \tan(\omega_n h) = \frac{k}{\upsilon}, \tag{15}$$

which must fall in the range

$$n\pi \leq \omega_n h \leq \left(n+\tfrac{1}{2}\right)\pi. \tag{16}$$

In addition, a parameter

$$\varepsilon_n = \frac{\sin(2\omega_n h)}{2\omega_n h} \quad \text{when } k \to \infty,\ \varepsilon_n \to 0, \tag{17}$$

has been introduced to reflect the slipping of each modal motion at the bottom.

In the above the notation $q_d(t, z; I_\tau)$ has been designed to represent the characteristic response of the drift current to the unit wind force I_τ. Similarly $q_s(t, z: I_\eta)$ means the characteristic response of the slope current to the unit slope force I_η. The two-letter variables *SE* and *BE* have been used to represent the wind-induced surface Ekman spiral and the slope-induced bottom Ekman spiral respectively.

Having determined the characteristic responses, we can obtain the response of the velocities to arbitrary forcing by performing a convolution in time:

$$q(t, z) = \nabla\eta(t) * \dot{q}_s(t, z; I_\eta) + \tau(t) * \dot{q}_d(t, z; I_\tau), \tag{18}$$

where the dots denote the time derivatives.

The Ekman dynamics has now been fully extracted. All its features, such as top and bottom Ekman layers, damped inertial oscillations with higher modes dying away faster, and the momentum diffusion e-folding time scale $(\delta_e^2/h^2 f)^{-1}$ (see equation (13)), are preserved analytically. The unknown $\nabla\eta(t)$ only affects the amplitude of the velocity profile (in a time convolution fashion).

As a consequence of the initial conditions in (3) and (4), we have

$$\sum_{n=0}^{\infty} a_n \cos(\omega_n z) = SE(z), \tag{19}$$

$$\sum_{n=0}^{\infty} c_n \cos(\omega_n z) = BE(z), \tag{20}$$

obtained by setting $t = 0$ in (5) and (6). In fact a_n and c_n given by (12) and (14) were calculated from these two relationships. Appendix I will use these two relations to accelerate the convergence of the velocity series.

2.2. *Characteristic responses in terms of transports*

Defining

$$[Q_d(t;\ I_\tau),\ Q_s(t;\ I_\eta)] = \int_{-h}^{0} [q_d(t,\ z;\ I_\tau),\ q_s(t,\ z;\ I_\eta)]\ dz \tag{21}$$

as the two characteristic transport responses induced by wind and sea surface slope respectively, substitution of (5) and (6) into the above yields

$$Q_d(t;\ I_\tau) = -i\frac{I_\tau}{f}\left(D_d - \sum_{n=0}^{\infty} E_n\ e^{-b_n t}\right), \tag{22}$$

$$Q_s(t;\ I_\eta) = i\frac{ghI_\eta}{f}\left(D_s - \sum_{n=0}^{\infty} G_n\ e^{-b_n t}\right), \tag{23}$$

where

$$D_d = 1 - \frac{1}{\cosh(\alpha h) + (\alpha\upsilon/k)\ \sinh(\alpha h)}, \tag{24}$$

$$D_s = 1 - \frac{1}{\alpha h}\frac{\tanh(\alpha h)}{1 + (\alpha\upsilon/k)\ \tanh(\alpha h)}, \tag{25}$$

$$E_n = \frac{4i\ \sin(\omega_n h)}{\omega_n h\left[(\omega_n h)^2(\delta_e/h)^2 + 2i\right](1 + \varepsilon_n)}, \tag{26}$$

$$G_n = \frac{4i\ \sin^2(\omega_n h)}{(\omega_n h)^2\left[(\omega_n h)^2(\delta_e/h)^2 + 2i\right](1 + \varepsilon_n)}. \tag{27}$$

The coefficients $-iI_\tau/f$ and $igh I_\eta/f$ on the RHS of (22) and (23) are the transport amplitudes, whose physical interpretations are the familiar steady Ekman transport and the geotrophic transport in deep water respectively. The quantities in parentheses are the corrections for the effects of bottom friction

and inertial acceleration. Again, as a result of the initial conditions in (3) and (4), there are two relationships:

$$\sum_{n=0}^{\infty} E_n = D_d, \tag{28}$$

$$\sum_{n=0}^{\infty} G_n = D_s. \tag{29}$$

These two relations will be used later to determine a proper mode number when a tolerance for truncation errors is given.

When the characteristics responses are known, the responses to arbitrary forcing can be calculated by

$$Q = \nabla\eta(t) * \dot{Q}_s(t;\ I_\eta) + \tau(t) * \dot{Q}_d(t;\ I_\tau). \tag{30}$$

2.3. *The difference form of the continuity equation and an η–Q lattice*

The continuity equation can be written in the form

$$\frac{\partial \eta}{\partial t} + \mathscr{R}\{\nabla^* Q\} = 0, \tag{31}$$

where

$$\nabla^* \equiv \frac{\partial}{\partial x} - i\,\frac{\partial}{\partial y} \tag{32}$$

and $\mathscr{R}$ denotes the real part. Q and η are coupled through the sea surface slope. We need to integrate the continuity equation (31) numerically and evaluate the transport (30) numerically step-by-step in time. Let us first discretize the continuity equation. The next subsection will discuss how to evaluate the transport given the updated value of $\nabla\eta$.

In differencing the above form of the continuity equation, an η–Q grid comes naturally (Figure 1), which is a counterpart of the Arakawa E-grid in the complex plane. Adopting the η–Q grid not only facilitates the calculation of $\nabla\eta$ for each Q-point but also automatically eliminates the spurious residual flow that occurs when one uses the Arakawa C-grid,[22] as will be shown in Figure 6. This is because, in contrast with the Arakawa C-grid, in the η–Q grid there is no need to average the Coriolis force over four neighbouring grid points.

Using an FTCS (forward in time and centred in space) scheme to discretize equation (31), one has

$$\eta_{l,m}^{(k+1)} = \eta_{l,m}^{(k)} - \mathscr{R}\left\{\left(Q_{l,m+1}^{(k)} - Q_{l,m-1}^{(k)}\right)s_x - i\left(Q_{l+1,m}^{(k)} - Q_{l-1,m}^{(k)}\right)s_y\right\}, \tag{33}$$

where $s_x = \Delta t/2\Delta x$, $s_y = \Delta t/2\Delta y$, the subscripts l and m denote the grid point indices and the superscript k denotes the kth time step.

2.4. *A recursion scheme for the time convolution*

For convenience the following notation is introduced: $R(t;\ 1)$ for the response of a linear system to unit force and $R(t;\ F)$ for the response to an arbitrary time-varying force F. Thus R can signify velocity response, transport response or bottom stress response, F can represent wind stress or sea surface slope

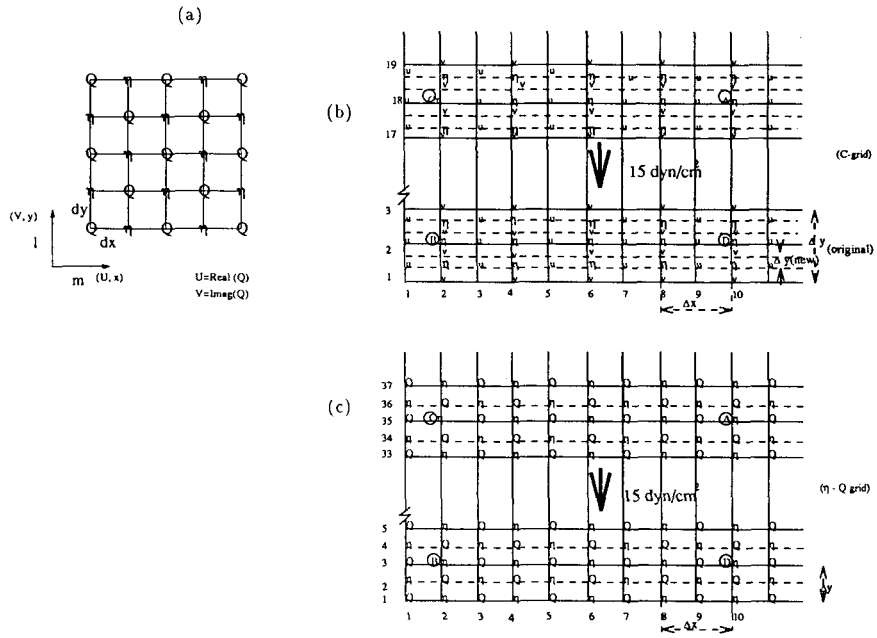

Figure 1. Panel (a) is an η–Q grid, a counterpart of the Arakawa E-grid in the complex plane, panel (b) is the C-grid used by Heaps[24] and panel (c) is the η–Q grid used in this model. Originally Heaps divided the basin horizontal plane into 35 × 19 lines (full lines in panel (b)) and marked four grid points for recording the model output. In the comparison tests Δys for both methods have been changed. One-half and one-third of Heaps' original Δy are used for the present method and Heaps' method respectively. By doing this, we can make the two methods have the same geometry co-ordinates for the four marked points while not letting Heaps method use the coarser grid size than the present one

and the recursion scheme to be derived will be suitable for any of these cases. The relationship between $R(t;\ F)$ and $R(t;\ 1)$ is given by

$$R(t;\ F) = \int_0^t F(t') \frac{\partial R(t - t';\ 1)}{\partial t}\, \mathrm{d}t'. \tag{34}$$

Numerical evaluation of this integral is necessary, since $F(t)$ is an arbitrary time function. Because t appears in both the integral limit and the integrand, the usual discrete summation for the integral would require recalculation of the summation from $t = 0$ for each time step. An economic evaluation scheme is thus needed and Jelesnianski[6] has provided one. However, both his derivation and his recursion scheme are complicated. This subsection gives a simple derivation for a simpler and physically clearer recursion scheme.

The structure of the solutions presented in (5), (6), (22) and (23) suggests that it is proper to write $R(t;\ 1)$ in the unified form

$$R(t;\ 1) = C(z) - \sum_{n=0}^{\infty} \phi_n(z)\, \mathrm{e}^{-b_n t}, \tag{35}$$

where $C(z)$ can be $(I_\tau/f\delta_e)SE(z)$, $i(qI_\eta/f)BE(z)$, $-i(I_\tau/f)D_d$ or $i(ghI_\eta/f)D_s$ and $\phi_n(z)$ can be $(I_\tau/f\delta_e)a_n \cos(\omega_n z)$, $i(gI_\eta/f)c_n \cos(\omega_n z)$, $-i(I_\tau/f)E_n$ or $i(ghI_\eta/f)G_n$. Since the initial response is set

to be zero (see (19), (20), (28) and (29)), we have

$$\sum_{n=0}^{\infty} \phi_n(z) = C(z) \tag{36}$$

(except at $z = 0$ when $R(t; 1)$ represents the stress). Substitution of (35) into (34) gives

$$\begin{aligned} R(t; F) &= \int_0^t F(t') \sum_{n=0}^{\infty} \phi_n(z) b_n \, \mathrm{e}^{-b_n(t-t')} \, \mathrm{d}t' \\ &= \sum_{n=0}^{\infty} r_n(t; F), \end{aligned} \tag{37}$$

where

$$r_n(t; F) = \int_0^t F(t') \phi_n(z) b_n \, \mathrm{e}^{-b_n(t-t')} \, \mathrm{d}t', \tag{38}$$

which denotes the response to an external force by the nth mode. For the next time step $t + \Delta t$ we have

$$\begin{aligned} R(t + \Delta t; F) &= \left(\int_0^t + \int_t^{t+\Delta t} \right) F(t') \sum_{n=0}^{\infty} \phi_n(z) b_n \, \mathrm{e}^{-b_n(t+\Delta t-t')} \, \mathrm{d}t' \\ &= \sum_{n=0}^{\infty} \left[r_n(t; F) \, \mathrm{e}^{-b_n \Delta t} + F(t) \phi_n(z) \left(1 - \mathrm{e}^{-b_n \Delta t}\right) \right], \end{aligned} \tag{39}$$

where in the first integral the result calculated at the previous time step has been used and in the second integral $F(t')$ has been approximated by $F(t)$ for $t' \in [t, t + \Delta t]$. Let us denote

$$r_n(t + \Delta t; F) = r_n(t; F) \, \mathrm{e}^{-b_n \Delta t} + F(t) r_n(\Delta t; 1), \tag{40}$$

where

$$r_n(\Delta t; 1) = \phi_n(z) \left(1 - \mathrm{e}^{-b_n \Delta t}\right), \tag{41}$$

which gives the response by the nth mode to a unit force in one time step. Then (39) can be written as

$$R(t + \Delta t; F) = \sum_{n=0}^{\infty} r_n(t + \Delta t; F). \tag{42}$$

Thus a recursion scheme for evaluating the response convolution is obtained. Starting from $r(0; F) = 0$ (be definition of (38)), one can use (40) to evaluate the response to an external force by each mode for successive time steps and then use (42) to obtain the total response. The scheme is summarized in the following box:

$$\begin{aligned} \lambda_n &= \mathrm{e}^{-b_n \Delta t}, \\ r_{nF}^{(0)} &= 0, \\ r_{n1}^{(1)} &= \phi_n(z)(1 - \lambda_n), \\ r_{nF}^{(k+1)} &= r_{nF}^{(k)} \lambda_n + F^{(k)} r_{n1}^{(1)}, \\ R_F^{(k+1)} &= \sum\nolimits_{n=0}^{N} r_{nF}^{(k+1)} \quad (k = 0, 1, 2, \ldots), \end{aligned} \tag{43}$$

where the notation $r_{nF}^{(k)}$ is short for $r_n(k\Delta t; F)$, $r_{n1}^{(1)}$ for $r_n(\Delta t; 1)$, etc., and N is a positive integer whose proper value will be discussed later.

A physical interpretation of the recursion scheme is as follows. The first term on the RHS of (40) (or the third equation of (43)) is due to the 'initial' condition at the previous time step and the second term is due to the latest 'kick' by the external force. $r_{n1}^{(1)}$ acts as a weight to partition the external force F into the nth modal motion. Since the frictional force has been taken care of in $r_{n1}^{(1)}$, one may read $F^{(k)}r_{n1}^{(1)}$ as a net force to drive the nth modal motion during the time interval $[k\Delta t, (k+1)\Delta t]$. The factor $e^{-b_n \Delta t}$ describes how each mode evolves once set into motion. Different modes evolve differently because of the different values of b_n ($n = 0, 1, 2, \ldots$).

The above recursion scheme can be applied to the response in velocity, stress and transport when one substitutes the corresponding $C(z)$, $\phi_n(z)$ and b_n. In terms of velocity the recursion scheme is expressed in Appendix I, where a discussion is also given on velocity convergence acceleration using relations (19) and (20). In terms of transport the recursion scheme is expressed as

$$
\begin{aligned}
&\lambda_n = \mathrm{e}^{-b_n \Delta t}, \\
&r_{nF}^{(0)} = 0\,, \\
&r_{n1r}^{(1)} = -\mathrm{i}\,\frac{I_\tau}{f}\,E_n(1-\lambda_n), \\
&r_{n1\eta}^{(1)} = \mathrm{i}\,\frac{ghI_\eta}{f}\,G_n(1-\lambda_n), \\
&r_{nF}^{(k+1)} = r_{nF}^{(k)}\lambda_n + r^{(k)}r_{n1r}^{(1)} + \nabla\eta^{(k)}r_{n1\eta}^{(1)}, \\
&Q^{(k+1)} = \sum\nolimits_{n=0}^{N} r_{nF}^{(k+1)} \quad (k = 0, 1, 2, \ldots),
\end{aligned}
\tag{44}
$$

where Q takes the place of R_F, and E_n and G_n are as given by (26) and (27) respectively. In programming (44), one should evaluate those k-independent quantities once before the updating 'do-loop'. Also, one can replace the symbols of unit wind stress I_τ and unit slope I_η in the programme by the number '1' so that the inputs τ and $\nabla\eta$ can automatically take care of the units and directions.

Now the formula for updating Q has been obtained, equations (33) and (44) form an explicit scheme for updating Q and η alternately. In various cases (different values of δ_e/h, flat or varying bottom topography, steady or unsteady wind, etc.) the numerical experimentation shows that the scheme is stable under the CFL condition $\Delta t \leq \Delta x\Delta y/\sqrt{[gh(\Delta x^2 + \Delta y^2)]}$ (the scheme is still stable even when the equal sign in the condition is taken). However, a theoretical stability analysis for the scheme is not available yet.

2.5. *Transfer of the zero-flux boundary condition to that for the surface elevation*

For an open lateral boundary condition one may use the Sommerfeld radiation condition to update η and Q based on information at neighbouring interior points at the previous time step (see e.g. Reference 23). For a solid lateral boundary the Q–η lattice introduced above requires that one calculates the surface gradient for Q-boundary points based on the fact that the flux normal to the wall is zero. Here let us focus on the transfer of the zero-flux condition to that for the surface gradient.

According to (44), $Q^{(k+1)}$ can also be written as

$$
Q^{(k+1)} = \sum_{n=0}^{N} r_{nF}^{(k)}\,\mathrm{e}^{-b_n \Delta t} + \tau^{(k)}R_{1\tau}^{(1)} + \nabla\eta^{(k)}R_{1\eta}^{(1)}, \tag{45}
$$

where

$$R_{1\tau}^{(1)} = \sum_{n=0}^{N} r_{n1\tau}^{(1)}, \tag{46}$$

$$R_{1\eta}^{(1)} = \sum_{n=0}^{N} r_{n1\eta}^{(1)}. \tag{47}$$

Letting

$$R_{1\eta}^{(1)} = a + \mathrm{i}b, \tag{48}$$

where a and b are both real, then

$$\nabla\eta^{(k)} R_{1\eta}^{(1)} = \left(a\,\frac{\partial\eta}{\partial x} - b\,\frac{\partial\eta}{\partial y}\right)^{(k)} + \mathrm{i}\left(a\,\frac{\partial\eta}{\partial y} + b\,\frac{\partial\eta}{\partial x}\right)^{(k)}. \tag{49}$$

Thus from (45), on a lateral boundary where $U = \mathscr{R}\{Q\}$ should be zero,

$$\frac{\partial\eta^{(k)}}{\partial x} = \frac{b}{a}\,\frac{\partial\eta^{(k)}}{\partial y} - \frac{1}{a}\,\mathscr{R}\left\{\sum_{n=0}^{N} r_{nF}^{(k)}\,\mathrm{e}^{-(\beta_n^2+\mathrm{i})f\,\Delta t} + \tau^{(k)} R_{1\tau}\right\}, \tag{50}$$

and on a lateral boundary where $V = \mathscr{I}\{Q\}$ should vanish,

$$\frac{\partial\eta^{(k)}}{\partial y} = -\frac{b}{a}\,\frac{\partial\eta^{(k)}}{\partial x} - \frac{1}{a}\,\mathscr{I}\left\{\sum_{n=0}^{N} r_{nF}^{(k)}\,\mathrm{e}^{-(\beta_n^2+\mathrm{i})f\,\Delta t} + \tau^{(k)} R_{1\tau}\right\}, \tag{51}$$

where $\mathscr{I}$ denotes the imaginary part of a complex quantity. In a corner where both U and V vanish,

$$\begin{bmatrix} \partial\eta/\partial x \\ \partial\eta/\partial y \end{bmatrix}^{(k)} = -\begin{bmatrix} a & -b \\ b & a \end{bmatrix}^{-1} \begin{bmatrix} \mathscr{R}\{\ldots\} \\ \mathscr{I}\{\ldots\} \end{bmatrix}^{(k)}, \tag{52}$$

where $\{\ldots\}$ is the same as that of (50) and (51).

2.6. *How large must N be?*

Let us come back to the expressions for the transports given in (22) and (23) to see how large a value of N is sufficient given a truncated error tolerance. Rewrite (22) and (23), with reference (28) and (29), in the form

$$\frac{Q_d(t;\, I_\tau)}{I_{Q_d}} = \left(\sum_{n=0}^{N} + \sum_{n=N+1}^{\infty}\right)(1 - \mathrm{e}^{-b_n t})E_n, \tag{53}$$

$$\frac{Q_d(t;\, I_\tau)}{I_{Q_s}} = \left(\sum_{n=0}^{N} + \sum_{n=N+1}^{\infty}\right)(1 - \mathrm{e}^{-b_n t})G_n, \tag{54}$$

where for brevity the notation I_{Q_d} and I_{D_s} has been introduced to represent the transport amplitudes $-iI_\tau/f$ and $ighI_\eta/f$ respectively. Truncation errors per I_{Q_d} and per I_{Q_s} may then be defined as

$$er_1 = \sum_{n=N+1}^{\infty} (1 - e^{-b_n t})E_n \approx \sum_{n=N+1}^{\infty} E_n, \tag{55}$$

$$er_2 = \sum_{n=N+1}^{\infty} (1 - e^{-b_n t})G_n \approx \sum_{n=N+1}^{\infty} G_n, \tag{56}$$

where b_n is as defined in (13). In the above definition the terms $e^{-b_n t}E_n$ and $e^{-b_n t}G_n$ have been dropped, because $\sum_{n=N+1}^{\infty} e^{-b_n t}E_n$ and $\sum_{n=N+1}^{\infty} e^{-b_n t}G_n$ approach zero much faster than do $\sum_{n=N+1}^{\infty} E_n$ and $\sum_{n=N+1}^{\infty} G_n$ respectively, so we need only consider the slowly convergent component to evaluate the truncation errors. Substitution of (26) and (27) into (55) and (56) yields

$$er_1 = \sum_{N+1}^{\infty} \frac{4i \sin(\omega_n h)}{(\omega_n h)\left[(\omega_n h)^2(\delta_e/h)^2 + 2i\right](1 + \varepsilon_n)}, \tag{57}$$

$$er_2 = \sum_{N+1}^{\infty} \frac{4i \sin(\omega_n h)}{(\omega_n h)^2\left[(\omega_n h)^2(\delta_e/h)^2 + 2i\right](1 + \varepsilon_n)}, \tag{58}$$

where $n\pi \leq \omega_n h \leq (n + \frac{1}{2})\pi$ (from (16)). From the above we see that the coefficients of the two error series decrease towards zero in orders of $1/n^3$ and $1/n^4$ $(n \geq N + 1)$ respectively. The first error corresponds to the wind-induced flow and the second to the sea-surface-slope-induced flow. For problems concerning purely slope-induced flow (such as tidal currents), N will be smaller for a given truncation error than for problems which include wind forcing. We also see that both truncation errors are inversely proportional to $(\delta_e/h)^2$. Thus we expect that N will be smaller in relatively shallow water (larger δ_e/h) than in deep water (smaller δ_e/h). This is because in shallow water the momentum versus depth distribution is more uniform owing to the stronger frictional effects, so fewer modes are needed to sum up the distribution.

The absolute values of the errors can also be calculated. Because of (28) and (29), we have from (55) and (56) that

$$|er_1| = \left| D_d - \sum_{n=0}^{N} E_n \right|, \tag{59}$$

$$|er_2| = \left| D_s - \sum_{n=0}^{N} G_n \right|, \tag{60}$$

with which one can quickly decide on a proper value of N for a given truncation error tolerance. For the case of a non-slip bottom condition ($k = \infty$) the absolute errors are tabulated in Table II and III as a function of N for different values of δ_e/h. These tables help to determine a proper mode number for a given error tolerance.

A complete description of the transport method for the case of constant eddy viscosity and constant density is now finished. A discussion on the extension of the method to the case of arbitrary depth-dependent eddy viscosity $\upsilon = \upsilon(z)$ and arbitrary density profile $\rho = \rho(x, y, z)$ is presented in Appendix II.

Table II. Truncated error per I_{Q_d} ($=I_\tau/f$, where I_τ is one unit of kinematic wind stress) when $t = 0$ for different values of δ_e/h and N. The truncated error is defined as $\varepsilon_N = \sum_{N+1}^{\infty}$

N	$\delta_e/h = 1$ $\lvert\varepsilon'\rvert \leq$	$\delta_e/h = 1/2$ $\lvert\varepsilon'\rvert \leq$	$\delta_e/h = 1/10$ $\lvert\varepsilon'\rvert \leq$	N	$\delta_e/h = 1$ $\lvert\varepsilon'\rvert \leq$	$\delta_e/h = 1/2$ $\lvert\varepsilon'\rvert =$	$\delta_e/h = 1/10$ $\lvert\varepsilon'\rvert =$
0	0·0319	0·1200	0·2734	8	0·0001	0·0003	0·0084
1	0·0062	0·0245	0·1495	9	0·0001	0·0003	0·0062
2	0·0021	0·0083	0·0955	10	0·0000	0·0002	0·0047
3	0·0009	0·0037	0·0614	11	0·0000	0·0001	0·0037
4	0·0005	0·0020	0·0392	12	0·0000	0·0001	0·0029
5	0·0003	0·0011	0·0254	13	0·0001	0·0001	0·0023
6	0·0002	0·0007	0·0170	14	0·0000	0·0001	0·0019
7	0·0001	0·0005	0·0118	15	0·0000	0·0001	0·0016

Table III. Truncated error per I_{Q_s} ($=igghI_\eta/f$, where I_η is one unit of sea surface slope) when $t = 0$ for different values of δ_e/h and N. The truncated error is defined as $\varepsilon_N = \sum_{N+1}^{\infty}$

N	$\delta_e/h = 1$ $\lvert\varepsilon''\rvert \leq$	$\delta_e/h = 1/2$ $\lvert\varepsilon''\rvert =$	$\delta_e/h = 1/10$ $\lvert\varepsilon''\rvert \leq$	N	$\delta_e/h = 1$ $\lvert\varepsilon''\rvert =$	$\delta_e/h = 1/2$ $\lvert\varepsilon''\rvert \leq$	$\delta_e/h = 1/10$ $\lvert\varepsilon''\rvert \leq$
0	0·0096	0·0365	0·1452	8	0·0000	0·0001	0·0018
1	0·0015	0·0061	0·0589	9	0·0000	0·0001	0·0013
2	0·0005	0·0019	0·0297	10	0·0000	0·0000	0·0010
3	0·0002	0·0008	0·0163	11	0·0000	0·0000	0·0008
4	0·0001	0·0004	0·0095	12	0·0000	0·0000	0·0006
5	0·0001	0·0003	0·0058	13	0·0000	0·0000	0·0005
6	0·0000	0·0002	0·0038	14	0·0000	0·0000	0·0004
7	0·0000	0·0001	0·0026	15	0·0000	0·0000	0·0003

3. TEST OF THE TRANSPORT METHOD IN HEAPS' BASIN

In this section the method described in the previous section is tested with some standard known results. Heaps'[24] rectangular basin with constant wind blowing and Heaps' spectral method are chosen for comparison. It is due to Heaps' pioneering work that the spectral method was introduced into oceanography to simulate 3D flows. The results from Heaps' work have been taken as a standard for comparison by most of the later spectral models (see e.g. References 11, 14, 15, 20, 25 and 26).

Heaps'[24] rectangular basin is 800 km long (north–south) and 400 km wide (east–west) (the basin geometry was chosen to mimic the North Sea). Heaps used the C-grid scheme to locate η- u- and v-points in a horizontal plane grid of 35 × 19 lines (Figure 1(b), full line), using

$$\Delta x = 400/9 \text{ km}, \qquad \Delta y = 800/17 \text{ km}, \tag{61}$$

and marked four η-points A, B, C and D for which the time series of the surface elevation and velocities (averaged over the four neighbouring points) are recorded. Since the η–Q grid scheme is used in the transport method, in order to locate the four η-points A, B, C and D in the grid plane with the same geometry as that of Heaps, a grid of 69 × 19 lines (Figure 1(b)) is placed on the horizontal plane for the transport method. In doing so, however, Heaps' method has to use a coarser grid size than the transport method. To avoid this, one-third of Heaps's original Δy is used as a new grid size for Heaps' method (Figure 1(b), broken line) in the tests.

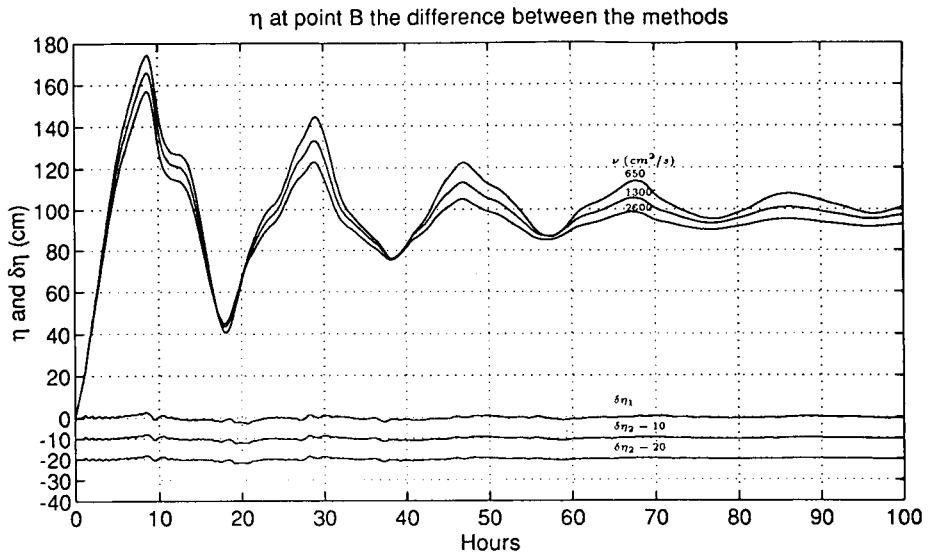

Figure 2. Time series of the surface elevation at point B for the first group of tests. Three elevation curves for different values of υ are generated by the transport method (using two modes) and compared with the same type of curves generated by Heaps' spectral method (using 10 modes). The differences between the two methods are shown by $\delta\eta_1$, $\delta\eta_2$ and $\delta\eta_3$ ($\delta\eta_1 = |\eta_T - \eta_H|$, where η_T is generated by the transport method and η_H by Heaps' method for $\upsilon = 650$ cm^2 s^{-1}, and so on; for clarity they are offset by -10 in the figure). The figure demonstrates that the transport method yields results in good agreement with Heaps' results (Parameters: $f = 1{\cdot}22 \times 10^{-4}$ s^{-1}, $g = 9{\cdot}81$ m s^{-2}, $\tau = -1{\cdot}5$ Pa, $\rho = 1{\cdot}025$ kg m^{-3}, $\Delta t = 6$ min, $h = 65$ m, $k = 0{\cdot}002$ m s^{-1}, $\upsilon = 0{\cdot}065$, $0{\cdot}13$, $0{\cdot}26$ m^2 s^{-1} ($\delta_e/h = 0{\cdot}50$, $0{\cdot}71$, $1{\cdot}00$), $\Delta x = 44{\cdot}44$ km, $\Delta y = 23{\cdot}52$ km for the transport method and $\Delta y = 15{\cdot}69$ km for the spectral method.)

Table IV. Illustration of the main idea of the transport approach

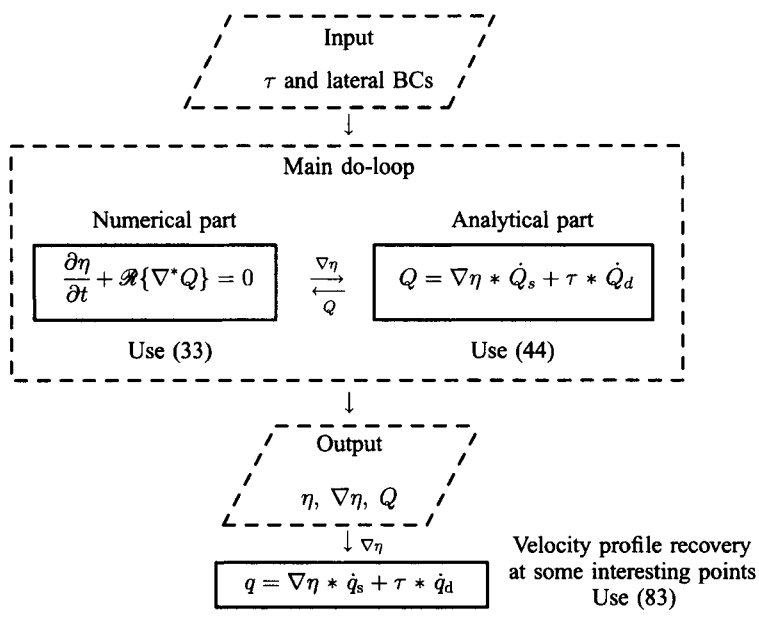

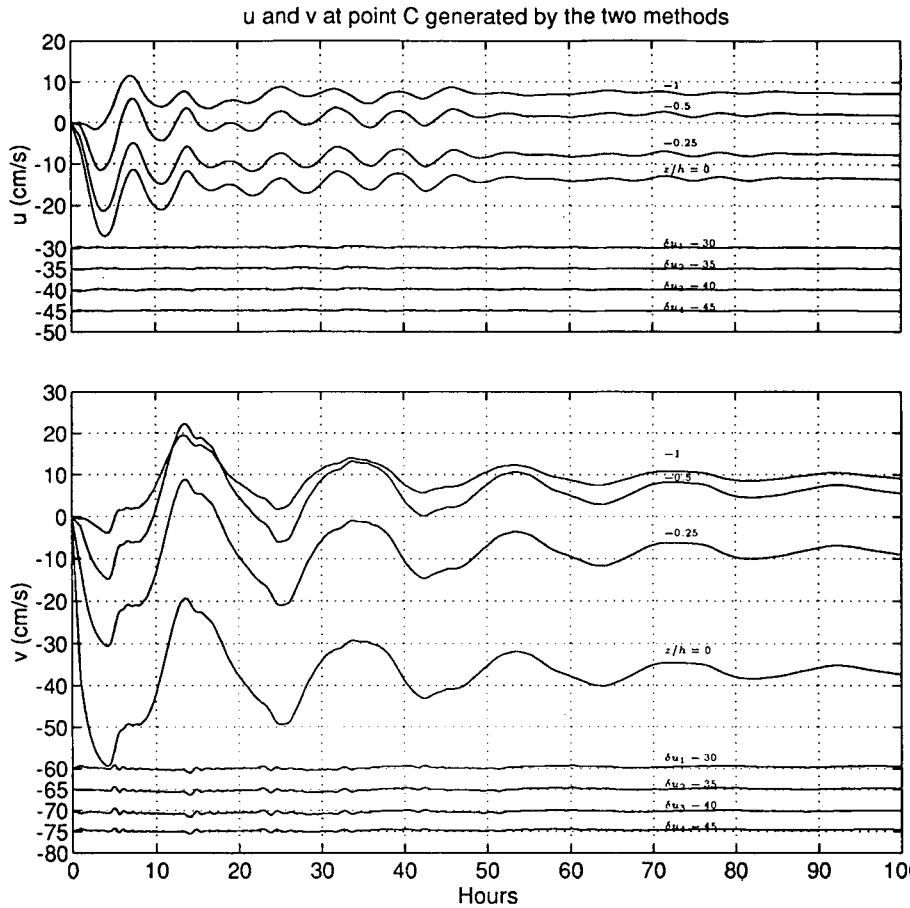

Figure 3. Velocity time series at four depths generated by the transport method (using two modes) and their difference from those generated by Heaps' method (using 10 modes). The differences are represented by δu_i and δv_i (i = 1, 2, 3, 4 for z/h = 0, −0·25, −0·5, −1) which are offset at different horizontal lines. The small difference shows that the transport method yields satisfactory results compared with Heaps' results (the parameters are the same as those in Figure 2 except for υ = 0·065 m^2 s^{-1} only)

Shown in Figure 2 are the three surface elevation time series at point B generated by the transport method using two modes. They are compared with those generated by Heaps' spectral method with 10 modes. (For Heaps' spectral model the 'wet point only' technique[22] has been used to avoid a spurious residual flow.) The difference between the two methods is represented by $\delta\eta_i$ (i = 1, 2, 3 for three values of υ; $\delta\eta_i = |\eta_T - \eta_H|_i$, where η_T represents η generated by the transport method and η_H by Heaps' spectral method). The figure demonstrates that the transport method works well and gives results that are very close to Heaps' results.

When the surface elevation field is obtained, the major part of the computation is finished. The velocity profiles at grid points of interest can be recovered using the record of $\nabla\eta$ at those points (Table (IV). Figure 3 shows velocities (using two modes) recovered at grid point C. The differences between the results of this method and Heaps' spectral method (using 10 modes) are represented by δu_i (i = 1, 2, 3, 4 for z/h = 0, −0·25, −0·50, −1; $\delta u = u_H - u_T$, where u_H denotes u generated by Heaps' method and u_T by the transport method) and δv_i (for clarity they are offset at different horizontal lines in the figure). The figure shows that the results yielded by the transport method are in satisfactory agreement with those by Heaps' method.

From the point of view of computational efficiency, the advantage of the transport method over Heaps' spectral method is clear: the transport method uses two modes while the spectral method uses 10 modes. This advantage will become more prominent when δ_e/h becomes smaller. Figures 4 and 5 compare the numbers of modes used by the transport method, Heaps' spectral method and a variation of Heaps' method[14] for $\delta_e/h = 0{\cdot}21$. The figures illustrate that Heaps' spectral method converges slowly both at the surface and at the bottom. Sheng and Thompson's method[14] effectively improves convergence at the surface but not at the bottom, while the transport method improves convergence at both the surface and the bottom. This is because the transport method extracts both the wind-induced surface Ekman spiral $SE(z)$ and the slope-induced bottom Ekman spiral $BE(z)$ from the series and so the remainder series converges exponentially (see the discussion in Appendix I and equation (83)). Heaps' method does not extract the Ekman spirals (however, he suggested a velocity correction to approximate the infinite summation, which is used in the tests here), which explains the slow convergence near the surface and bottom. Sheng and Thompson's method extracts only the wind-induced surface Ekman spiral; the slope-induced bottom Ekman spiral is left in the series. Therefore

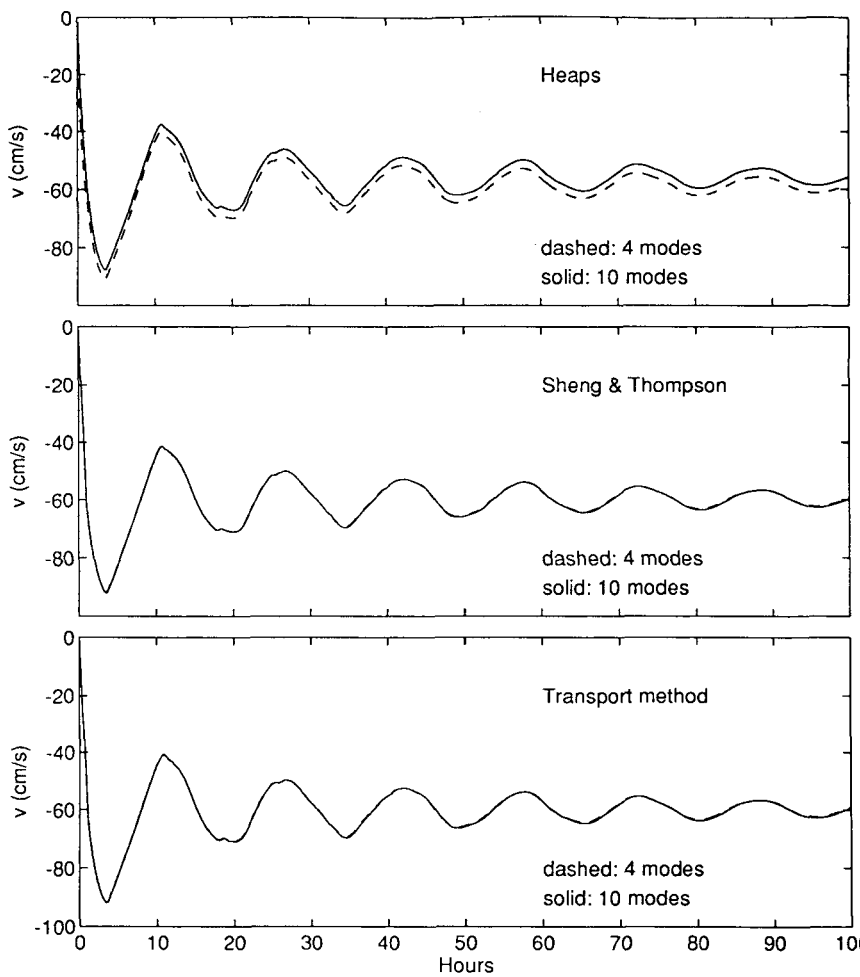

Figure 4. Comparison of the convergence rates at the surface ($z/h = 0$) for the three methods in the Heaps basin (Except for $h = 100$ m, $\upsilon = 0{\cdot}026$ m^2 s^{-1} and $k = 0{\cdot}004$ m s^{-1} ($\delta_e/h = 0{\cdot}21$) the parameters are the same as those in Figure 2.)

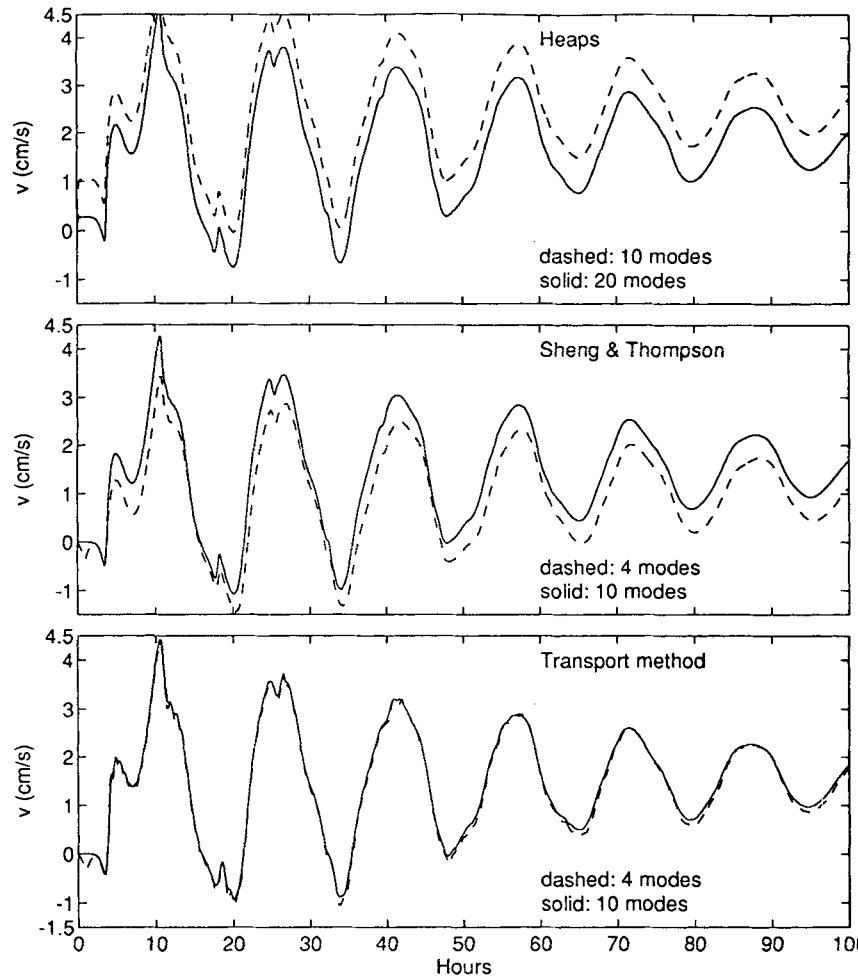

Figure 5. Comparison of the convergence rates at the bottom ($z/h = -1$) for the three methods in the Heaps basin (Except for $h = 100$ m, $\upsilon = 0{\cdot}026$ m^2 s^{-1} and $k = 0{\cdot}004$ m s^{-1} ($\delta_e/h = 0{\cdot}21$) the parameters are the same as those in Figure 2.)

their method still converges slowly near the bottom. A more theoretical comparison of the transport method with the others will be presented in the next section.

For Heaps' rectangular basin problem an analytical solution for η and $q(z)$ in the steady state can be found. The transport should be zero everywhere in the steady state because of the flat bottom and the uniform wind field. Thus from (22) and (23) one can deduce a relationship between the ultimate sea surface slope and the wind stress, namely

$$\nabla\eta^{(\infty)} = \frac{D_d}{D_s}\frac{\tau}{gh}, \tag{62}$$

which is a constant over the entire basin. Thus the ultimate sea surface is a plane and can be described by

$$\eta = \mathscr{R}\left\{\frac{D_d}{D_s}\frac{\tau}{gh}\right\}x + \mathscr{I}\left\{\frac{D_d}{D_s}\frac{\tau}{gh}\right\}y + c, \tag{63}$$

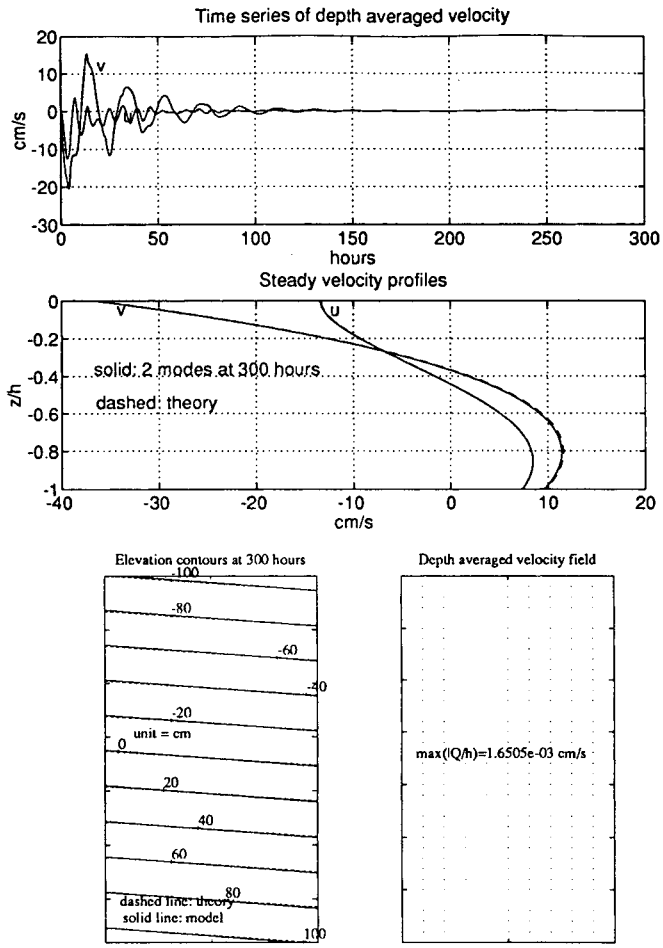

Figure 6. The top panel shows the vanishing depth-averaged velocity. The middle and bottom panels are a comparison between the theoretical steady state (represented by broken lines) and the model output at 300 h after the constant wind is set up over the Heaps basin. Two modes are used both in updating η and Q in the main do-loop and in recovering the velocity profile afterwards. This figure also shows that in the transport method there is no problem of undamped inertial oscillation or spurious residual flow

in which the constant c can be determined by the fact that the surface at the middle point of the basin should be zero owing to the conservation of water mass and the symmetry in the basin geometry. For example, if the origin of the co-ordinate is at the centre of the basin, then $c = 0$. The ultimate velocity profile can be calculated by

$$q^{(\infty)} = \frac{\tau}{f\delta_e}\left(SE(z) + i\frac{\delta_e}{h}\frac{D_d}{D_s}BE(z)\right). \tag{64}$$

Jamart and Ozer[22] obtained the steady solutions only up to the knowledge of the sea surface slope and the velocity profiles. Here the use of the simple fact that the sea surface plane should go through the zero point at the centre of the basin completely determines the whole steady solution. Equations (62)–(64) are useful in the sense that every new algorithm proposed for spectral methods is first tested in Heaps' basin.

Figure 6 shows a comparison between the theoretical steady state (represented by broken lines) and the model output of 300 h after the constant wind is set up (represented by full lines). As one can see, the agreement between the theoretical prediction and the model calculation is satisfactory. The top panel of the figure is the time series of the depth-averaged velocity, showing that there are no undamped inertial oscillations[10,13] with the transport approach. The bottom panel also shows that adopting the η–Q grid (a counterpart of the Arakawa E-grid in the complex plane) automatically eliminates the spurious residual flow problem.[22]

4. A COMPARISON OF THE TRANSPORT APPROACH, THE BOTTOM STRESS APPROACH AND THE SPECTRAL METHOD

To solve the linearized equations of motion (as given by (1)), we have three closely related methods at our disposal: the spectral method as well as two approaches based on the convolution method, namely the bottom stress approach and the transport approach. These focus on three related but different expansions. The spectral method employs a velocity expansion of the form

$$q \sim \Sigma A_n \cos(\omega_n z), \tag{65}$$

in which the A_n are updated at each time step by solving a set of modal equations. In this sense the spectral method may also be classified as a velocity approach. The bottom stress approach employs a bottom stress expansion which is a vertical derivative of (65). The transport approach employs a transport series which is a vertical integral of (65). Thus the three approaches are relevant in the sense that they all deal with the same family of series, but different in the sense that they pick different family members, as summarized in Table V.

When comparing the convergence rates of two trigonometric series, it is the usual practice to compare the rates at which their coefficients approach zero (see e.g. Reference 27, pp. 144–145; in the following discussion, terms such as 'rate', 'speed', 'fast' and 'slow' are to be understood in this sense). Now suppose that

$$\frac{A_n}{n^{-p}} = \text{constant as } n \to \infty, \tag{66}$$

which means that A_n *and* $1/n^p$ are of the same order, where p is a positive number. From (12), (14) and (16) one can deduce immediately that $p = 2$ when wind is present and $p = 3$ when only sea surface

Table V. Relevance and difference of the three approaches (for the format of the series listed for the velocity recovery see (83) and for a_n and c_n see (12) and (14))

	Transport approach (this study)	Velocity approach (Heaps[24])	Bottom stress approach (Jelesnianski[6])	
Series involved in the main do-loop	—	$A_n \cos(\omega_n z)$	—	(velocity)
	$\Sigma \frac{A_n}{\omega_n} \sin(\omega_n h)$	$\Sigma \frac{A_n}{\omega_n} \sin(\omega_n h)$	$\Sigma \frac{A_n}{\omega_n} \sin(\omega_n h)$	(transport) (stress)
	—	—	$\Sigma A_n \omega_n \sin(\omega_n h)$	
Series involved in the velocity recovery	$\Sigma(a_n, c_n)\, e^{-b_n \Delta t} \cos(\omega_n z)$	—	$\Sigma(a_n, c_n)\, e^{-b_n \Delta t} \cos(\omega_n z)$	

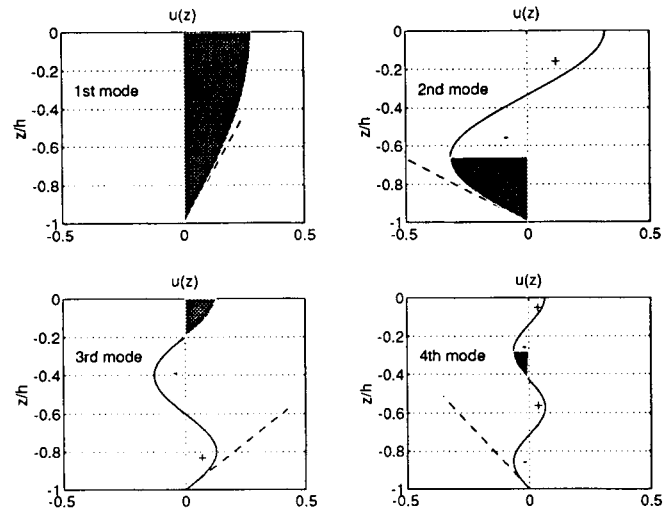

Figure 7. This diagram illustrates why the transport series converges most quickly. The net transport due to each mode is represented by the shaded area and the bottom stress by the broken line. The transport in this example is mainly due to the first and second modes; higher modes contribute little to the transport but may significantly contribute to the velocity and even more to the bottom stress (The curves shown here are for the velocities of each mode based on the second part of q_d when $t = 0$, $\delta_e/h = \frac{1}{2}$ and $k = \infty$.)

slope forcing is present. Then, because $\omega_n h \sim n$, we have

$$\frac{A_n/\omega_n h}{n^{-(p+1)}} = \text{constant} \quad \text{as } n \to \infty \tag{67}$$

for the transport series

$$\frac{A_n/\omega_n h}{n^{-(p-1)}} = \text{constant} \quad \text{as } n \to \infty \tag{68}$$

for the bottom stress series. Thus the coefficients of the transport series decrease one order faster than those of the velocity series and two orders faster than those of the stress series. Figure 7 illustrates this graphically.

From Table V we can see that the transport approach decouples quickly convergent series from the slower series, while the other approaches couple two series. When a calculation process involves the summation of two series simultaneously, the convergence rate is controlled by the slowly convergent series, i.e. in the velocity approach and stress approach the calculation for the elevation is slowed down by the calculation of the velocity and bottom stress respectively. The transport method has no such problem and can let the calculation for the elevation proceed at its own speed. After the elevation calculation is completed, the transport approach employs the analytical formula (18) to recover the velocity. The main advantage in using the analytical formula is that the formula extracts both the wind-induced surface Ekman spiral and the slope-induced bottom Ekman spiral so that the remainder can converge exponentially (see (5), (6), (83) and Table IV).

There are two additional advantages in using the analytical formula. First, one can use a different time step from that used in the main do-loop. For an explicit scheme the time step in the main do-loop, say Δt_M, is restricted by the CFL condition and can be very small when the water is very deep. In this case one might consider using a multiple of Δt_M as the time step for the velocity calculation. Figure 8 shows the effects on the velocity recovery of using a different time step as well as a different number of modes. Second, there are many practical cases which only require that the velocity profile be calculated

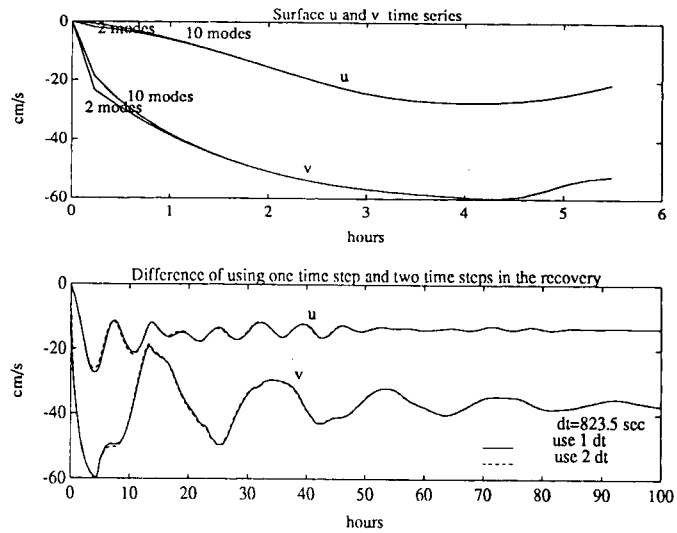

Figure 8. Since the transport method separates the calculation for the transport and elevation from that for the velocity, it is permissible to use a different number of modes and a different time step in the velocity recovery. This can be an advantage in reducing the computational workload in some cases. This figure shows the effects of using a different number of modes and a different time step (Note that because of the factor $e^{-b_n \Delta t}$ ($b_n \sim n^2$), the value of N is also affected by the choice of Δt. In a slow-varying problem a large value of Δt can be chosen and the value of N can be reduced accordingly given a fixed truncation error. In a fast-changing problem a small value should be chosen for Δt and thus the value of N should be increased. The transport method is flexible enough to accommodate these needs.)

at a few grid points rather than at every grid point. The transport approach allows one to calculate the velocity profiles at only the points of interest. In contrast, the velocity approach (spectral method) requires calculation of the velocity profiles at every grid point whether they are needed or not. Any one of these three advantages results in a great saving of computational workload, while their combination saves even more. The bottom stress shares the same advantages in the velocity recovery, but it needs the greatest number of modes in the main do-loop since it employs the slowest series.

Another feature of the transport approach is that it solves only one equation numerically (the continuity equation) rather than three. Thus the numerical task is made easier. Lynch and Werner[28], and Lynch *et al.*[29] proposed a method for solving the 3D linearized equations of motion which essentially also solves a single Helmholtz-like equation for η. However, an arbitrary time dependence motion is replaced by a single harmonic motion in their work. In this work there is no restriction on the time dependence of the motion; the forcing function can be arbitrary.

5. COMMENTS ON THE VELOCITY-SPLIT FORM IN THE SPECTRAL METHOD

The purpose of this study is to implement Welander's transport approach. However, one point warrants further discussion, which is closely related to the recent efforts to improve the convergence of the spectral method for the velocity profile. It was found that Heaps' classical spectral method converges too slowly (see e.g. Reference 15 and 26) near the surface when there is non-zero wind stress on the surface. Recent efforts to accelerate the convergence have split the velocity into two parts—a prescribed component and a remainder series—whose coefficients need to be updated by numerically solving a set of modal equations

$$q = \Psi(z) + \sum A_n \cos(\omega_n z). \tag{69}$$

The convergence rate of the remainder series depends strongly on the choice of form for $\Psi(z)$. Various authors[14–18] have proposed different forms of $\Psi(z)$.

A general format for all the previously proposed forms can be written as

$$\Psi(z) = F_s\Psi_s(z) + F_b\Psi_b(z), \tag{70}$$

where Ψ_s and Ψ_b are two prescribed profiles and F_s and F_b are two depth-independent quantities, usually related to the surface stress and bottom stress respectively.

An alternative expression for (18) is

$$q = \frac{\tau(t)}{f\delta_e} SE(z) + \frac{ig\nabla\eta(t)}{f} BE(z) - \sum_{n=0}^{\infty}\left(\frac{a_n}{f\delta_e}\frac{\partial\tau}{\partial t} + c_n\frac{ig}{f}\frac{\partial\nabla\eta(t)}{\partial t}\right) * e^{-b_n t}\cos(\omega_n z). \tag{71}$$

This form suggests that a more suitable form for $\Psi(z)$ is

$$\Psi(z) = \frac{\tau(t)}{f\delta_e} SE(z) + i\frac{g\nabla\eta(t)}{f} BE(z), \tag{72}$$

where $SE(z)$ and $BE(z)$ are as given by (7) and (8) respectively or can be numerically obtained for an arbitrary eddy viscosity $\upsilon(z)$. In a system such as Heaps' basin, which permits a steady state eventually, this form is optimal; when t is sufficiently large, any other form of $\Psi(z)$ will cause the remainder series to contain a non-vanishing part, i.e.

$$\sum A_n\cos(\omega_n z) = \frac{\tau}{f\delta_e} SE(z) - F_s\Psi_s(z) + i\frac{g\nabla\eta}{f} BE(z) - F_b\Psi_b(z). \tag{73}$$

In other words, the difference between (70) and (72) is buried in the remainder series. Given a truncation error tolerance, one needs to sum a certain number of modes to get this buried part no matter how much time passes. If one chooses (72) for $\Psi(z)$, then one will not need any mode to sum when t is sufficiently large.

For time-dependent states, since the external forces $\tau(t)$ and $\nabla\eta(t)$ can be arbitrary functions of time, let us turn to considering single-frequency forcing. Conclusions from the single-frequency study should be illuminating for arbitrary forcing, since the latter can be decomposed into different frequency modes. Thus assume harmonic time dependences,

$$\tau(t) = \tau e^{i\sigma t}, \tag{74}$$

$$\nabla\eta(t) = \nabla\eta e^{i\sigma t}, \tag{75}$$

after which combination of (71) and (69) gives

$$\begin{aligned}\sum_{n=0}^{\infty} A_n\cos(\omega_n z) = {} & \frac{\tau e^{i\sigma t}}{f\delta_e} SE(z) - F_s\Psi_s(z) + i\frac{g\nabla\eta(t)e^{i\sigma t}}{f} BE(z) - F_b\Psi_b(z)\\ & - \sum_{n=0}^{\infty}\frac{i\sigma}{i\sigma + b_n}\left(a_n\frac{\tau e^{i\sigma t}}{f\delta_e} + c_n\frac{ig}{f}\nabla\eta e^{i\sigma t}\right)\cos(\omega_n z)\\ & + \sum_{n=0}^{\infty}\frac{i\sigma}{i\sigma + b_n}\left(a_n\frac{\tau e^{i\sigma t}}{f\delta_e} + c_n\frac{ig}{f}\nabla\eta e^{i\sigma t}\right)e^{-b_n t}\cos(\omega_n z)\\ & - \sum_{n=0}^{\infty}\left(a_n\frac{\tau}{f\delta_e} + c_n\frac{ig}{f}\nabla\eta\right)e^{-b_n t}\cos(\omega_n z).\end{aligned} \tag{76}$$

This equation provides a means for theoretical assessment of all the previously proposed forms under the basis functions $\{\cos(\omega_n z)\}$ which are the eigenfunctions of problems (3) and (4). If one choses (72) for $\Psi(z)$, one will find (with reference to (12)–(16)) that the coefficient of the remainder series is described by

$$A_n \sim \max\left(\frac{\sigma/f}{n^4}, \frac{\sigma/f}{n^5}, \frac{e^{-n^2 t}}{n^2}, \frac{e^{-n^2 t}}{n^3}\right) \tag{77}$$

(in which the first and third terms are related to the wind forcing and the second and fourth terms to the pressure gradient forcing). When $t > 0$, the last two terms in parentheses approach zero exponentially as $n \to \infty$, leaving the first term (or the second term when $\tau(t) = 0$) as the controlling term. Substituting all the previously proposed forms[14–18] in (76) reveals that

$$A_n \sim \frac{1}{n^3}. \tag{78}$$

Thus the form (72) is preferable to the others as a prescribed part of the velocity under the basis of the eigenfunctions of problems (3) and (4). (For other basis functions, e.g. $\{\cos[(n\pi/h)z]\}$, which are not the eigenfunctions of problems (3) and (4) when $k \neq 0$, whether this preference still holds needs further investigation.) The form of (72) requires calculation of $\nabla\eta$ at each velocity grid point. It will be difficult to perform this calculation with the Arakawa C-grid but will be easy with the Arakawa E-grid. The numerical experiment of this study adopts the E-grid. The E-grid not only brings this study good agreement with the results from using the C-grid but also automatically eliminates the spurious residual flow problem.

6. CONCLUSIONS

Regarding the pressure gradient force in the two linearized momentum equations as a local external force, one can easily obtain two characteristic responses of the local Eulerian velocity. These characteristic responses can be analytically expressed in terms of unit constant wind stress and unit constant pressure gradient. The coefficients in the expression, however, may either have an analytical relationship with the mode number n and the system parameters $(\delta_e/h, k)$ or only have numerical values, depending on the arbitrariness of the eddy viscosity profile $\upsilon(z)$ and the density profile $\rho(z)$. The response to the arbitrary wind and pressure forcing can be obtained by convolving these two forces with the time derivatives of the two characteristic responses. Thus a full velocity profile $q(t, z; \nabla\eta, \tau)$ is analytically extracted. Our knowledge of the system would be complete if $\eta(t, x, y)$ (hence $\nabla\eta(t, x, y)$) were known. Thus the key point becomes how to find the solution for $\eta(t, x, y)$. To get $\eta(t, x, y)$, the transport method numerically solves the continuity equation (where the transport is supplied by the depth integration of the velocity profile) instead of solving a set of depth-averaged equations of motion. By doing so, the numerical task is reduced, since only one equation needs to be finitely differenced and integrated, and more importantly the convergence rate is enhanced, since high modes do not contribute to the transport as significantly as they do to the velocity or the bottom stress.

ACKNOWLEDGEMENTS

The author wishes to thank Drs. A. J. Bown, K. R. Thompson, D. Wright and D. Walsh for their reading the manuscript and providing comments. This study is supported by the Natural Science and Engineering Research Council of Canada.

APPENDIX I: VELOCITY RECURSION SCHEME AND ACCELERATION OF VELOCITY CONVERGENCE USING EQUATIONS (19) AND (20)

The recursion scheme (43) can apply to the response in velocity, stress and transport when one substitutes the corresponding $C(z)$, $\phi_n(z)$ and b_n. In terms of velocity the recursion scheme is expressed as

$$\begin{aligned}
&\lambda_n = \mathrm{e}^{-b_n \Delta t},\\
&r_{nF} = 0,\\
&r_{n1\tau} = \frac{I_\tau}{f\delta_e} a_n \cos(\omega_n z)(1-\lambda_n),\\
&r_{n1\eta} = \mathrm{i}\frac{gI_\eta}{f} c_n \cos(\omega_n z)(1-\lambda_n),\\
&r_{nF}^{(k+1)} = r_{nF}^{(k)}\lambda_n + \tau^{(k)} r_{n1\tau} + \nabla\eta^{(k)} r_{n1\eta},\\
&q^{(k+1)} = \sum_{n=0}^{N} r_{nF}^{(k+1)} \quad (k = 0, 1, 2, \ldots),
\end{aligned} \tag{79}$$

where q takes the place of R_F in (43) and a_n and b_n are as given by (12) and (13).

As we can see from the above, in the summation of the series

$$\sum_{n=0}^{\infty} r_{nF}^{(k+1)} \tag{80}$$

the convergence rate is controlled by the series

$$\sum_{n=0}^{\infty} a_n \cos(\omega_n z), \qquad \sum_{n=0}^{\infty} c_n \cos(\omega_n z) \tag{81}$$

rather than

$$\sum_{n=0}^{\infty} a_n \cos(\omega_n z)\lambda_n, \qquad \sum_{n=0}^{\infty} c_n \cos(\omega_n z)\lambda_n. \tag{82}$$

The latter converges much faster than the former, since the factor λ_n decreases exponentially as n increases. We obviously want to take advantage of this fact. This can be achieved by using the relationship of (19) and (20) to extract the slowly converging parts from the summations. Thus we can

derive the following quickly convergent scheme for the velocity recovery:

$$
\begin{aligned}
&\lambda_n = \mathrm{e}^{-b_n \Delta t},\\
&r_{nF} = 0,\\
&r_{n1\tau} = \frac{I_\tau}{f\delta_e}\, a_n\, \cos(\omega_n z)(1-\lambda_n),\\
&r_{n1\eta} = \mathrm{i}\,\frac{gI_\eta}{f}\, c_n\, \cos(\omega_n z)(1-\lambda_n),\\
&R_{1\tau} = \frac{I_\tau}{f\delta_e}\left(SE(z) - \sum\nolimits_{n=0}^{N} a_n\, \cos(\omega_n z)\lambda_n\right),\\
&R_{1\eta} = \frac{gI_\eta}{f}\left(BE(z) - \sum\nolimits_{n=0}^{N} c_n\, \cos(\omega_n z)\lambda_n\right),
\end{aligned}
\tag{83}
$$

$$
\begin{aligned}
q^{(k+1)} &= \sum\nolimits_{n=0}^{N} r_{nF}^{(k)}\lambda_n + \tau^{(k)}R_{1\tau} + \nabla\eta^{(k)}R_{1\eta},\\
r_{nF}^{(k+1)} &= r_{nF}^{(k)}\lambda_n + \tau^{(k)}r_{n1\tau} + \nabla\eta^{(k)}r_{n1\eta} \quad (k = 0,\ 1,\ 2,\ \ldots).
\end{aligned}
$$

APPENDIX II: EXTENSION OF THE APPROACH

The two characteristic velocity responses are obtained under the assumption of constant eddy viscosity and constant density. In this appendix we discuss the extension of the transport approach to the cases of arbitrary but time-invariant eddy viscosity $\upsilon(z)$ and density anomaly $\rho = \rho_0[1 + \varepsilon(x, y, z)]$.

AII.1 The case of arbitrary depth-dependent $\upsilon(z)$

When $\upsilon = \upsilon(z)$, the formal solution (e.g. equation (5) or (6)) for the characteristic velocity repsonse still holds:

$$
q(t,\ z;\ I) = C(z) - \sum_{n=0}^{\infty} A_n \mathrm{e}^{-\left(\beta_n^2 + i\right)ft} Z_n(z), \tag{84}
$$

where $C(z)$ is a steady current (wind-induced or slope-induced), Z_n and β_n are eigenfunctions and eigenvalues values defined by

$$
\frac{\partial}{\partial z}\left(\upsilon(z)\,\frac{\partial Z}{\partial z}\right) = -f\beta_n^2 Z, \tag{85}
$$

$$
\left.\frac{\partial Z}{\partial z}\right|_{z=0} = 0, \qquad Z|_{z=-h} = 0 \tag{86}
$$

and A_n are Fourier coefficients with the respect to the eigenfunctions. The steady velocity $C(z)$ should be easy to obtain by numerical integration. If the eigenfunctions and eigenvalues are known, then the Fourier coefficients A_n can be obtained by numerical evaluation of

$$
A_n = \frac{1}{\|\cdot\|}\int_{-h}^{0} C(z)Z(z)\,\mathrm{d}z, \tag{87}
$$

where $\| \cdot \|$ denotes the norm of Z_n, and (84) can be evaluated and the characteristic responses in velocity determined. Therefore the crux here is how to solve the Sturm–Liouville eigenvalue problem given by (85) and (86). When $\upsilon(z)$ is of some proper form, such as a linear function, exponential, power, etc., there exist various analytical solutions[30] to (85) and (86). What is needed here is a numerical solution of the eigenvalue problem where $\upsilon(z)$ does not admit an analytical solution.

Davies solved the eigenvalue problem using a Galerkin method by expanding each of the eigenfunction in terms of a set of B-spline functions[26] or alternatively by using the Runge–Kutta–Merson iteration method.[31] In the following a direct way of solving the problem is presented. Without loss of generality let us consider the following form of the eigenfunction problem:

$$(\upsilon Z')' = -\lambda Z, \tag{88}$$

$$Z'(0) = 0, \qquad Z(-1) = 0 \tag{89}$$

which can be regarded as non-dimensional forms of (85) and (86). Dividing $[-1, 0]$ into $n - 1$ equal parts and applying centred differences on (88) results in

$$AZ = -\lambda Z, \tag{90}$$

where

$$A = \frac{1}{(\Delta z)^2} \begin{bmatrix} -\upsilon_{5/2} & \upsilon_{5/2} & 0 & 0 & \cdots & 0 \\ \upsilon_{3/2} & a_2 & \upsilon_{5/2} & 0 & \cdots & 0 \\ 0 & \upsilon_{5/2} & a_3 & \upsilon_{7/2} & \cdots & 0 \\ \vdots & \vdots & \ddots & \ddots & \ddots & \vdots \\ 0 & 0 & \cdots & \upsilon_{n-3/2} & a_{n-1} & \upsilon_{n-1/2} \\ 0 & 0 & \cdots & 0 & \upsilon_{n-1/2} & a_n \end{bmatrix}, \tag{91}$$

$$a_i = -(\upsilon_{i-1/2} + \upsilon_{i+1/2}) \quad (\text{for } i = 2, \ldots, n), \tag{92}$$

$$Z = [Z_1 \; Z_2 \; \ldots \; Z_n]^T, \tag{93}$$

with $[Z_1 \; Z_2 \; \ldots \; Z_n]$ being a set of eigenfunction values evaluated at $[z_1 \; z_2 \; z_3 \; \ldots \; z_n]$. Thus the Sturm–Liouville problem has been turned into a matrix eigenvalue problem. An introduction to this numerical method of solving Sturm–Liouville problems can be found in Reference 32.

For illustration, a computational example is supplied in which the eddy viscosity profile is specified in two layers and the analytical solutions for the eigenvalues and eigenfunctions were obtained by Heaps.[33,34] Figure 9 is a comparison of the first five eigenfunctions calculated analytically and numerically, and the eddy viscosity profile is also shown; the numerical solution of the eigenvalue problem gives a satisfactory approximation to the analytical one. Also, we can see that the bottom logarithmic layer is well-resolved.

AII.2 The case of non-uniform density field $\rho = \rho_0[1 + \varepsilon(x, y, z)]$

In this case there will be an extra component, say q', compared with the case of barotropic pressure and constant eddy viscosity, in the characteristic velocity response contributed by the baroclinic pressure force, described by

$$\frac{\partial q'}{\partial t} + ifq' = -g\nabla\eta_d(x, y, z) + \upsilon \frac{\partial^2 q'}{\partial z^2}, \tag{94}$$

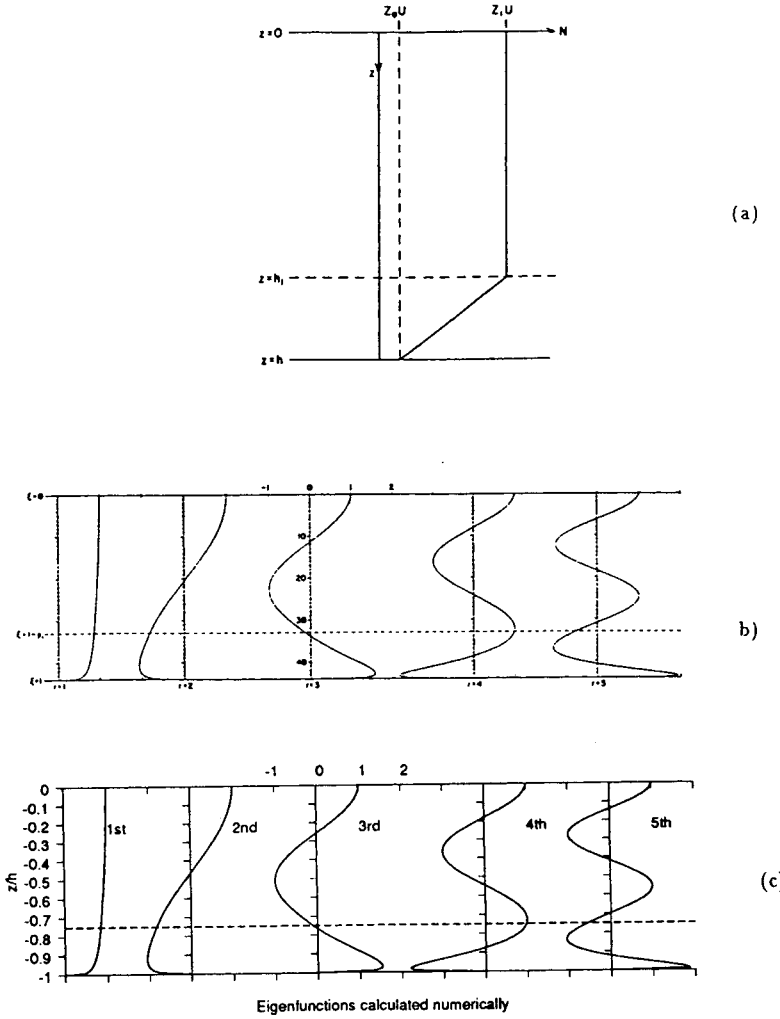

Figure 9. The top panel is the eddy viscosity used by Heaps[33,34], and the middle panel shows the first five eigenfunctions obtained analytically by Heaps. The bottom panel shows the first five eigenfunctions calculated numerically using the method described in the text

where

$$\eta_d = \int_z^0 \varepsilon \, dz, \tag{95}$$

subject to the same boundary conditions as those in (4). The solution can be found from

$$q' = C'(z) - \sum_{n=0}^{\infty} A_n \, e^{-(\beta_n^2 + i)ft} \cos(\omega_n z), \tag{96}$$

where

$$A_n = \frac{2}{h} \int_{-h}^{0} C'(z) \cos(\omega_n z) \, dz \tag{97}$$

and $C'(z)$ is a steady solution of (94), which can be found by using, say, the Green function method. The transport approach introduced above can then be followed.

REFERENCES

1. P. Welander, 'Wind action on a shallow sea: some generalizations of Ekman's theory,' *Tellus*, **IX**, 45–52 (1957).
2. P. Welander, 'Numerical prediction of storm surges', in H. E. Landsberg and J. Van Mieghem (eds), *Advances in Geophysics*, Vol. 8, Academic, New York, 1961, pp. 316–379.
3. G. W. Platzman, 'The dynamical prediction of wind tides on Lake Erie', in *Meteorological Monographys*, Vol. 4, American Meteorological Society, 1963, pp. 1–44.
4. T. J. Simons, *Canadian Bulletin of Fisheries and Aquatic Sciences, Circulation Models of Lakes and Inland Seas*, Vol. 203, 1980.
5. T. S. Murty, *Canadian Bulletin of Fisheries and Aquatic Sciences*, Vol. 212, *Storm Surges*, Vol. 203, 1984.
6. C. P. Jelesnianski, 'Bottom stress time-history in linearized equations of motion for storm surges,' *Mon. Weather Rev.*, **98**, 462–478 (1970).
7. G. Z. Forristall, 'Three-dimensional structure of storm-generated currents', *J. Geophys. Res.*, **79**, 2721–2729 (1974).
8. G. Z. Forristall, 'Continental shelf currents in tropical storm Delia: Observations and theory', *J. Phys. Oceanogr.*, **7**, 532–546 (1977).
9. G. Z. Forristall, 'A two-layer model for hurricane-driven currents on an irregular grid,' *J. Phys. Oceanogr.*, **10**, 1417–1437 (1980).
10. A. M. Davies, *Spectral Models in Continental Shelf Sea Oceanography*, American Geophysical Union, Washington, DC, 1987, pp. 245–255.
11. A. M. Davies, 'On formulating two-dimensional vertical integrated hydrodynamic numerical models with an enhanced representation of bed stress', *J. Geophys. Res.*, **93**, 1241–1263 (1988).
12. C. J. Hearn and J. R. Hunter, 'A new method of describing bottom stress in two-dimensional hydrodynamical models of shallow homogeneous seas, estuarines, and lakes', *Appl. Math. Modell.*, **12**, 573–580 (1988).
13. C. J. Hunter and J. R. Hearn, 'The single relaxation approximation for bottom stress in two-dimensional hydrodynamic models of shallow seas', *Continental Shelf Res.*, **9**, 465–478 (1989).
14. J. Sheng and K. R. Thompson, 'A modified Galerkin–spectral model for three-dimensional, barotropic, wind-induced shelf circulation', *J. Geophys. Res.*, **98**, 7011–7022 (1993).
15. R. W. Lardner, 'Numerical solution of the linearized three-dimensional tidal equations using eddy viscosity eigenfunctions', *J. Geophys. Res.*, **95**, 22,269–22,274 (1990).
16. T. Zitman, 'Quasi three-dimensional current modelling based on a modified version of Davies' shapefunction approach', *Continental Shelf Res.*, **12**, 143–157 (1992).
17. A. M. Davies, 'Solution of the 3D linear hydrodynamic equations using an enhanced eigenfunction approach', *Int. j. numer. methods fluids*, **13**, 235–250 (1991).
18. A. M. Davies, 'Modelling currents in highly sheared surface and bed boundary layers', *Continental Shelf Res.*, **12**, 189–211 (1992).
19. J. Pedlosky, *Geophysical Fluid Dynamics*, Springer, New York, 1979.
20. R. W. Lardner and H. M. Cekirge, 'A new algorithm for three-dimensional tidal and storm surge computations', *Appl. Math. Modell.*, **12**, 471–571 (1988).
21. R. W. Lardner, 'A vertical/horizontal splitting algorithm for the three-dimensional tidal and storm surge computations', *Proc. R. Soc. Lond. A*, **430**, 263–283 (1990).
22. B. M. Jamart and J. Ozer, 'Numerical boundary layers and spurious residual flows', *J. Geophys. Res.*, **91**, 10,621–10,631 (1986).
23. D. C. Chapman, 'Numerical treatment of cross-shelf boundaries in a barotropic coastal ocean model', *J. Phys. Oceanogr.*, **15**, 1060–1075 (1985).
24. N. S. Heaps, 'On the numerical solution of the three dimensional hydrodynamic equations for tides and storm surges', *Mem. Soc. R. Sci. Liege, Ser. 6*, 143–180 (1971).
25. A. M. Davies and A. Owen, 'Three dimensional numerical sea model using the Galerkin method with a polynomial basis set', *Appl. Math. Modell.*, **3**, 421–428 (1979).
26. A. M. Davies, 'Formulation of a linear three-dimensional hydrodynamic sea model using a Galerkin–eigenfunction method', *Int. j. numer. methods fluids*, **3**, 33–60 (1983).
27. G. P. Tolstov, *Fourier Series*, Prentice-Hall, Englewood Cliffs, NJ, 1962.
28. D. R. Lynch and F. E. Werner, 'Three-dimensional hydrodynamics on finite elements. Part I: Linearized harmonic model,' *Int. j. numer. methods fluids*, **7**, 871–909 (1987).
29. D. R. Lynch, F. E. Werner, D. Greenberg and J. W. Loder, 'Diagnostic model for baroclinic, wind-driven and tidal circulation in shallow seas', *Continental Shelf Res.*, **12**, 37–64 (1992).
30. T. F. Jordan and J. R. Baker, 'Vertical structure of time-dependent flow dominated by friction in a well-mixed fluid', *J. Phys. Oceanogr.*, **10**, 1091–1103 (1980).

31. A. M. Davies, 'On the determination of vertical structure functions for time-dependent flow problems', *Tellus A*, **38**, 462–477 (1986).
32. D. Zwillinger, *Handbook of Differential Equations*, Academic, New York, 1989.
33. N. S. Heaps, 'Three-dimensional model for tides and surges with eddy viscosity prescribed in two layers. I: Mathematical formulation', *Geophys. J. R. Astron. Soc.*, **64**, 291–302 (1981).
34. N. S. Heaps, 'Three-dimensional models for tides and surges with vertical eddy viscosity prescribed in two layers., II: Mathematical formulation', *Geophys. J. R. Astron. Soc.*, **64**, 303–320 (1981).